Westra, Seth Pieter; Sisson, Scott A. Detection of non-stationarity in precipitation extremes using a max-stable process model. Journal of Hydrology, 2011; 46(1-2):119-128

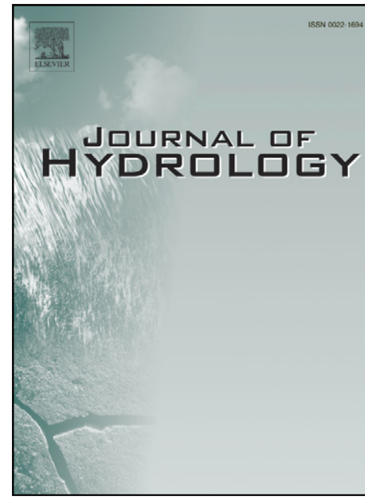

Detection of non-stationarity in precipitation extremes using a max-stable process model

Seth Westra, Scott A. Sisson

PII: S0022-1694(11)00411-2
DOI: 10.1016/j.jhydrol.2011.06.014
Reference: HYDROL 17701

To appear in: *Journal of Hydrology*

Received Date: 21 December 2010
Revised Date: 4 May 2011
Accepted Date: 15 June 2011

Detection of non-stationarity in precipitation extremes using a max-stable process model

Seth Westra[1] and Scott A. Sisson[2]

[1]Water Research Centre, School of Civil and Environmental Engineering, University of New South Wales, Australia

[2]School of Mathematics and Statistics, University of New South Wales, Australia

[1] Non-stationarity in extreme precipitation at sub-daily and daily timescales is assessed using a spatial extreme value model based on max-stable process theory. This approach, which was developed to simulate spatial fields comprising observations from multiple point locations, significantly increases the precision of a statistical inference compared to standard univariate methods. Applying the technique to a field of annual maxima derived from 30 sub-daily gauges in east Australia from 1965 to 2005, we find a statistically significant increase of 18% for 6-minute rainfall over this period, with smaller increases for longer duration events. We also find an increase of 5.6% and 22.5% per degree of Australian land surface temperature and global sea surface temperature at 6-minute durations, respectively, again with smaller scaling relationships for longer durations. In contrast, limited change could be observed in daily rainfall at most locations, with the exception of a statistically significant decline of 7.4% per degree land surface temperature in southwest Western Australia. These results suggest both the importance of better understanding changes to precipitation at the sub-daily timescale, as well as the need to more precisely simulate temporal variability by accounting for the spatial nature of precipitation in the statistical model.

1. Introduction

[2] The question of how extreme precipitation will change under a future climate represents an urgent research problem, not least because of the significant societal impacts that would result from an increase in precipitation-induced flooding [*Wilbanks et al.*, 2007]. To better constrain future projections, an important line of evidence comes from statistical assessments of changes to extreme precipitation in the observational record, with a large number of such studies recently having been published [e.g. *Alexander et al.*, 2006; *Frich et al.*, 2002; *Groisman et al.*, 2005]. These studies, which typically focus on the detection of trends from daily gauged precipitation data, find increases in extremes throughout most of the world including in many locations where mean annual precipitation is decreasing, with these changes generally being of similar sign but greater in magnitude than expected from climate

model simulations [*Allan and Soden*, 2008; *Allan et al.*, 2010]. Nevertheless, there remains significant uncertainty associated with quantifying long-term trends from these limited observational records [*O'Gorman and Schneider*, 2009], particularly for smaller spatial domains and at sub-daily timescales.

[3] Despite the obvious importance of such observational studies, surprisingly little attention has been given in the climate literature to the development of statistical methods that are able to provide inference on observed changes in extremes at the necessary levels of precision. In particular, assuming by way of example that extreme precipitation will scale at a rate of 7%/°C in proportion to the water holding capacity of the atmosphere [*Min et al.*, 2009; *O'Gorman and Schneider*, 2009; *Trenberth et al.*, 2003], and considering a global warming trend over the 20th century of about 0.74°C [*IPCC*, 2007], methods of detection would need to be sensitive to changes in the order of only 5% over the historical record. Univariate methods applied to point precipitation data generally are not appropriate in this context: when analysing the statistical power of four approaches to modelling trends in extreme rainfall (including annual maxima and *r*-largest maxima approaches from extreme value theory), Zhang *et al* [2004] found that such trends would be detected at the 5% significance level in less than 20% of cases [see also *Frei and Schar*, 2001].

[4] To address these deficiencies, many studies use extreme precipitation indices based on averaging over either space or time, in an effort to increase the signal-to-noise ratio and thus improve the detectability of any trends which might be present. For example, based on climate model outputs, Hegerl et al. [2004] find that anthropogenic influences in precipitation can be best detected in an index representing the averages of the 5 or 10 wettest days of the year, with changes to rarer events being more difficult to detect. Similarly, numerous studies have pooled data from multiple locations across some spatial domain [e.g. *Alexander et al.*, 2006; *Fowler and Wilby*, 2010; *Groisman et al.*, 2005] in order to improve statistical inference, with Min et al. [2009] finding that trends in extreme precipitation might become detectable when pooling data to global or hemispheric scales. Difficulties with this approach, however, include differences in scale (in particular it is often unclear how to standardise the data prior to averaging, with different approaches likely to yield different outcomes) and the development of correct inferential techniques, particularly in the presence of spatial correlation between the original gauged data. Furthermore, local-scale information is lost by

pooling the data in this manner, particularly in terms of the marginal distributions of the original point-based gauged data.

[5] A more elegant solution involves fitting a spatial extreme value model to multiple point locations within the spatial domain of interest, accounting for both the spatial and temporal variability in model parameters as well as the dependence between individual point-based records [e.g. see discussion in *Aryal et al.*, 2009; *Frei and Schar*, 2001; *Katz*, 2010]. The natural class of model to simulate such data is known as a max-stable process [*de Haan*, 1984; *de Haan and Pickands*, 1986; *Resnick*, 1987], which in terms of asymptotic motivations can be directly regarded as the spatial analogue of the univariate generalised extreme value (GEV) distribution. The max-stable model differs from the more commonly used "spatial GEV" model, in which univariate GEV parameters are modelled as a function of spatial location and potentially other covariates. The spatial GEV typically assumes spatial independence of the precipitation process conditional on the model parameters [*Buishand*, 1991], which can lead to unrealistic spatial inference and prediction [see *Katz et al.*, 2002 for a discussion of this issue, and Section 2.1 of this paper for an example of the implicaitons of ignoring data-level spatial dependence].

[6] Although much of the theory for multivariate max-stable models was derived over 20 years ago, computational challenges and the absence of a proper inferential framework for analysing spatial extremes have provided a significant barrier to the wider uptake of the method [e.g. see *Coles*, 1993; *Smith*, 1990 for early work on fitting max stable process models]. However, standard likelihood-based fitting techniques have recently been developed [*Padoan et al.*, 2010], paving the way for their routine implementation in applied research.

[7] This study provides one of the first applications of a max-stable process model to simulate both spatial and temporal variability, using a synthetic dataset and two different sets of observational records of annual maximum precipitation in Australia. The objectives of the synthetic study are to highlight the benefits of fitting a spatial model to multiple point locations, assess the implications of spatial dependence between data, and answer the question: how much data is required to derive a given level of inference? Two Australian precipitation datasets are used to demonstrate this model in the detection and attribution of temporal change. The first is the east-Australian sub-daily (pluviograph) precipitation record, which is of interest due to the recent evidence that changes to extremes are most likely to be found in short-duration precipitation events [*Haerter et al.*, 2010; *Hanel and Buishand*, 2010;

Hardwick-Jones et al., 2010; *Lenderink and van Meijgaard*, 2008], the importance of sub-daily rainfall for urban drainage and flood estimation [*Berne et al.*, 2004] and the abovementioned difficulties associated with detecting change from short observational records. The second dataset is a longer record of daily-read gauges located throughout Australia, and is used as an independent dataset for comparison with the pluviograph record, while also providing additional information at locations where pluviograph data is unavailable.

[8] The remainder of the paper is structured as follows. In the following section a brief overview is provided of the max-stable process methodology, followed by a synthetic study which highlights the benefits of using the technique in the detection of trends. In Section 3 we present the data used in the analysis, comprising both daily-read and pluviograph records across Australia. The results are then presented in Section 4, followed by conclusions in Section 5.

2. Methodology

[9] In this section we provide a description of max-stable process models and the relevant statistical fitting procedures, before presenting a synthetic study to assess how much data is required to result in a particular level of statistical significance of trend detection in extremes, as related to the strength of spatial dependence between point locations.

2.1 Models for spatial extremes

[10] Classical univariate extreme value theory describes the statistical behaviour of $M_n = \max\ \{X_1, \ldots, X_n\}$ for large *n*, where $X_1, X_2, \ldots$ is a sequence of independent (or weakly dependent) observations having a common distribution function [e.g. *Leadbetter et al.*, 1983]. For example, X_t might represent the daily precipitation recorded at a particular rain gauge on day *t*, and if *n=365* then M_n would correspond to the annual maximum daily rainfall [e.g. *Coles*, 2001]. Asymptotic results state that under some regularity conditions (such as continuity of the underlying distribution function of X_t), normalising sequences $\{a_n\}$ and $\{b_n > 0\}$ can be found such that

$$\Pr\left(\frac{M_n - a_n}{b_n} \leq z\right) \rightarrow G(z)$$

as $n \to \infty$, for a non-degenerate distribution function G. It follows [e.g. *Jenkinson*, 1955; *von Mises*, 1954] that G belongs to the Generalized Extreme Value (GEV) family, with distribution function

$$G(z) = \exp\left\{-\left[1 + \xi\left(\frac{z-\mu}{\sigma}\right)\right]^{-1/\xi}\right\},$$

defined on the set $\{z: 1 + \xi(z-\mu)/\sigma > 0\}$, where μ and $\sigma > 0$ are location and scale parameters respectively. The shape parameter, ξ, determines the type of tail behaviour: $\xi < 0$, $\xi = 0$ and $\xi > 0$ correspond to the Weibull, Gumbel (in the limit as $\xi \to 0$) and Fréchet sub-families of distributions respectively.

[11] Although the above theory applies in the general case only in the limit as $n \to \infty$, in practice this result allows the GEV distribution to be substituted as an approximation to the actual distribution of observed block maxima for finite n. For example, the GEV distribution could be used to model the annual maximum daily rainfall over a number of years [*Coles et al.*, 2003]. The unknown normalisation constants, $\{a_n\}$ and $\{b_n > 0\}$, may be absorbed into the model parameters, which can then be estimated through standard statistical procedures such as maximum likelihood [*Coles*, 2001; *Sisson et al.*, 2006], probability-weighted (L-weighted) moments [*Hosking et al.*, 1985; *Kharin and Zwiers*, 2000; *Perkins et al.*, 2009] or Bayesian inference [*Coles et al.*, 2003]. Predictions of future maxima at the point location can then be made via inversion of the distribution function. Extreme value modelling via GEV distributions has had much application in the hydrological sciences (see above references). See e.g. Leadbetter et al. [1983], Resnick [1987] and Coles [2001] for further discussion and alternative representations of extreme value models.

[12] The statistical theory and practice of univariate extremes is well developed. However many environmental processes have a natural spatial domain. Several authors have proposed modelling spatially dependent extremes through hierarchical models [e.g. *Sang and Gelfand*, 2007; *Zhao and Chu*, 2010], whereby dependence between neighbouring sites is achieved by enforcing strong relationships between the GEV parameters at each site. However, this approach typically assumes that the data are conditionally independent given the parameters, and as such, the models are unable to account for data-level dependence unless this is explicitly built into the model. For example, under a stationary environmental process (whereby the GEV parameters are constant at each site) prediction under the spatial GEV model effectively assumes independent predictions at each spatial location. Hence an

observed 1 in 100-year event (such as a storm) occurring simultaneously over two closely neighbouring spatial locations will predicatively occur under the spatial GEV model once in every 100×100 years - a serious underestimate. One alternative approach for modelling spatial extremes that naturally accounts for spatial data-level dependence is through max-stable processes.

[13] Max-stable processes are a spatial analogue of multivariate extreme value models [*de Haan*, 1984; *de Haan and Pickands*, 1986; *Resnick*, 1987] - a direct extension of the univariate GEV model into the spatial domain, which goes beyond the limitations of the spatial GEV model. Max-stable processes provide a general framework for modelling multivariate extremes with spatial and temporal dependence [*Coles*, 1993; *Padoan et al.*, 2010; *Smith*, 1990]. In analogy with the univariate theory, suppose that $\{X_i(s)\}_{s\in S}$ for $i = 1, \ldots, n$ are now n independent realisations of a continuous process indexed by s, where $S \subseteq \mathbb{R}^2$ commonly represents the bivariate spatial domain. As before, if the limit

$$\tilde{X}(s) = \lim_{n\to\infty} \frac{\max\limits_{i=1,\ldots,n} X_i(s) - a_n(s)}{b_n(s)}$$

exists for all $s \in S$, with normalising constants $a_n(s)$ and $b_n(s) > 0$, then $\tilde{X}(s)$ is a max-stable process [*de Haan*, 1984]. It follows [*de Haan and Resnick*, 1977] that for a fixed point in space, s, each one-dimensional marginal distribution belongs to the univariate GEV family, and that any K-dimensional marginal distribution (i.e. for multiple locations, s) belongs to the class of multivariate extreme value distributions. In practice, this means that the resulting parameters $\mu(s)$, $\sigma(s) > 0$ and $\xi(s)$ are now continuous spatial functions to be estimated. However, unlike spatial GEV models, the max-stable process naturally permits modelling and prediction with data-level spatial dependence.

[14] A useful interpretation of stationary max-stable processes (e.g. with unit Fréchet one-dimensional "GEV" margins) is the storm profile model [*Schlather and Tawn*, 2003; *Smith*, 1990]. This is based on a Poisson process $\{Y_j, U_j\}_{j\geq 1}$ of "storms" centred at $Y_j \in \mathbb{R}^2$ with magnitude $U_j > 0$, where each storm has a shape governed by a non-negative, measurable function $f(y - s)$ such that $\int_{\mathbb{R}^2} f(y - s)dy = 1$ for fixed $s \in S$. For example, f could be a Gaussian density function [*Smith*, 1990]. If these storms are observed from a fixed location in space, s, the maximum observed event at that location is given by

$$Z(s) := \max_{j\geq 1}\{U_j f(Y_j - s)\}, \quad s \in S.$$

The process, $Z(s)$, defines a stationary max-stable process. An illustration of this idea in one and two dimensions is given in **Figure 1** based on a Gaussian storm profile. **Figure 1(a)** displays $n = 5$ independent "storm" realisations, with the resulting process maxima highlighted (black line). The process maxima is not itself a realisation from a max-stable process as this requires $n \to \infty$ (suitably scaled) realisations. Similarly to univariate GEV models, the max-stable process limit can be used to approximate the distribution of the process maxima as n gets large. **Figure 1(b)** shows a realisation of a two-dimensional max-stable process. In both images, it is clear that two locations separated by a spatial distance within the range of the storm profile will tend to exhibit closely related data observations.

INSERT FIGURE 1 HERE

[15] Given a series of n observed data points $X_{i,k}$ for $i = 1, \ldots, n$ at K spatial locations $s^1, \ldots, s^K \in S$, the aim of a statistical analysis would be to fit a max-stable process using assumed parametric (or non-parametric) forms for the parameters $\mu(s)$, $\sigma(s) > 0$ and $\xi(s)$, while also estimating spatial dependence through the storm profile, f. However, for more than $K = 2$ spatial locations, the distribution function of the general max-stable process has no analytically tractable form [e.g. *Padoan et al.*, 2010], which thereby presents a problem for flexible and practical statistical model fitting through e.g. standard likelihood methods, and so ad-hoc procedures are usually adopted [e.g. *Smith*, 1990].

[16] When considering exactly $K = 2$ spatial locations, a bivariate class of spatial models with locations s^i and $s^j \in \mathbb{R}^2$ is available when the storm profile model, f, is a bivariate Gaussian density [*de Haan and Pereira*, 2006; *Smith*, 1990]. In this case the bivariate distribution function of $\{Z(0), Z(h)\}$ is

$$\Pr\left(Z(0)\leq z_i, Z(h)\leq z_j\right)=\exp\left[-\frac{1}{z_i}\Phi\left(\frac{a(h)}{2}+\frac{1}{a(h)}\log\frac{z_j}{z_i}\right)-\frac{1}{z_j}\Phi\left(\frac{a(h)}{2}+\frac{1}{a(h)}\log\frac{z_i}{z_j}\right)\right],$$

where $h = \left(s^j - s^i\right)'$, 0 is the origin, Φ is the standard univariate Gaussian distribution function, $a(h) = (h'\Sigma^{-1}h)^{1/2}$ and Σ is the (unknown) covariance matrix of f. From the above, the density function of $\{Z(0), Z(h)\}$ may be derived [e.g. *Padoan et al.*, 2010]. Note that $a(h)$ measures the strength of extremal dependence between s^i and s^j: $a(h) \to 0$

indicates complete dependence and $a(h) \to \infty$ represents complete independence [*de Haan and Pereira*, 2006]. A general max-stable process with a Gaussian storm profile, f, is known as a Gaussian extreme value process [*Smith*, 1990]. An alternative analytically tractable bivariate distribution function, based on a different storm process, is given by Schlather [2002].

[17] In order to model more than $K = 2$ spatial locations, Padoan et al [2010] proposed a pairwise composite likelihood approach. Here an approximate likelihood function is constructed as a product of density terms for each pair of locations s^i and s^j, $i \neq j$, where the density is derived from the distribution function of $\{Z(0), Z(h)\}$, above. Subject to suitable regularity conditions [*Padoan et al.*, 2010], the maximum likelihood estimate of the pairwise composite likelihood provides consistent and unbiased parameter estimates and confidence intervals, when the standard maximum likelihood estimate of the full (but intractable) max-stable likelihood model is unavailable. Perhaps most usefully, as this approach is likelihood-based, the usual suite of statistical techniques become available (suitably modified to account for the model mis-specification), resulting in a powerful and flexible inferential framework. For example, it is then trivial to build in e.g. regression-based forms for the parameters $\mu(s)$, $\sigma(s) > 0$ and $\xi(s)$ and estimate spatial dependence parameters (e.g. Σ). See Padoan et al [2010] for further details, and the accompanying code for model fitting in the *R* statistical programming language.

2.2 Detecting trends in extremes: spatial dependence and sample size

[18] We now present a synthetic study to assess the effect of spatial dependence and the length of the observed data record in statistically detecting location trends in extremes. We commence with a univariate analysis, where the data are drawn from a non-stationary GEV distribution with a linear temporal trend so that $\mu(t) = \beta_0 + \beta_1 t$, with $t = 0, \ldots, (n-1)$, where the indexing of the parameter μ is now with respect to time. The remaining parameters are fixed at $\sigma = 1$ and $\xi = 0$, with $\beta_0 = 1$, unless stated otherwise. The aim is to determine the value of β_1 which can be found to be statistically significant at the 5% significance level.

[19] Throughout this study, parameters are estimated using maximum likelihood, with the univariate models implemented using the *R* package "*ismev*" (http://www.r-project.org/) [see also *Coles*, 2001] and max-stable model with composite likelihoods through the *R* package "*SpatialExtremes*" [*Padoan et al.*, 2010]. For each setting, a total of 10,000 replicates were

generated, each of n observed sample points, and confidence intervals of the linear trend parameter β_1 were estimated using the profile likelihood, as described by [*Coles*, 2001]. The probability of detecting a trend was estimated as the proportion of the 10,000 replicates for which the trend parameter was statistically significantly different from zero at the 5% significance level. This is a practically useful means of presenting the results, as one often wishes to know the probability of being able to detect a trend of given magnitude from an observational record of finite length.

[20] The value of the trend coefficient, β_1, that can be detected with 50%, 95% and 99% probability is shown in **Figure 2(a)** as red solid, dashed and dotted lines, respectively, as a function of the observed sample length n. As expected, the statistical power increases with the sample length, so that smaller trends are detectable with larger datasets, with this increase being approximately linear on a log-log scale. Furthermore, there also is a clear relationship between the size of the β_1 coefficient and the probability of being able to detect this trend at a given significance level (here 5%). For example, if it is desirable to have a 99% probability of detecting a significant trend at the 5% significance level, it would be necessary to have nearly twice the sample length (n) than if one would be satisfied with only a 50% probability of detecting that trend. This type of reasoning becomes important when identifying data requirements for studies into the detection of trends.

INSERT FIGURE 2 HERE

[21] The influence of different values of ξ is also shown in **Figure 2(a)** (solid lines) for a 50% probability of trend detection; this information is plotted in more detail in **Figure 2(b)**. As can be seen, the greater the absolute value of ξ, the lower the value of β_1 that can be detected at a given significance level, with this becoming particularly noticeable for larger values of $|\xi|$. This occurs as holding the scale parameter fixed (at $\sigma = 1$) results in observed data that are more clustered around the location (μ) for increasing $|\xi|$, than for $\xi = 0$, thereby allowing more precise estimates of the location coefficients. As will be discussed further in Section 4, in the present analysis we find values of ξ on average slightly positive (~0.17) with a range of between -0.1 and 0.4 depending on the specific site. With sample sizes of 41 (sub-daily gauges) and 96 (daily gauges), such an average value of ξ would allow for an approximately 5% smaller value of β_1 to be detected compared to the case where $\xi = 0$.

[22] We now consider the influence of estimating a trend using a number of spatial locations, assuming a fixed record length of $n = 100$ at each site. The data was generated at *K* random locations within a unit square, under both the case of spatial independence (i.e. using the spatial GEV model) as well as including different degrees of spatial dependence (i.e. using the max-stable process model). Without loss of generality we assumed identical marginal parameters across the spatial domain (i.e. $\mu(t) = \beta_0 + \beta_1 t$ with $\beta_0 = 1$, $\sigma = 1$ and $\xi = 0$).

[23] **Figures 2(c)** and **(d)** show the values of β_1 that have a 50% and 95% probability, respectively, of being detected as a statistically significant trend (at the 5% level), as a function of the number of spatial locations, *K*. In the case of spatial independence, the results are qualitatively similar to the case of increasing sample length n: namely, the value of β_1 that can be detected at the 5% level decreases linearly as the number of spatial locations increases. This is an obvious consequence of using more data. However, for a fixed number of spatial locations, the presence of spatial dependence effectively reduces the amount of independent data in the sample, thereby increasing the value of β_1 that can be detected. The value of β_1 which can be detected at a given probability decreases more slowly with greater dependence, highlighting that the inclusion of spatial information is most beneficial when dependence is low. Interestingly, the rate of decrease of β_1 is approximately an order of magnitude lower for adding spatial information compared with temporal information. This clearly highlights that although spatial information significantly increases signal detectability, it remains a poor substitute for increasing length of record when this information is available.

[24] Having demonstrated the advantages of explicitly considering spatial information in the detection and attribution of trends in extremes, we now apply the max-stable process model to the annual maxima of daily and sub-daily precipitation at different locations in Australia. The data used for this analysis is described below.

3. Data

[25] Two alternative precipitation datasets were used in this analysis. The first was a subset of Australia's pluviograph record, which provides measurements of precipitation in increments of 6 minutes at 1397 locations around Australia [see description in *Westra et al.*, 2010]. For this study we considered only near-complete data over the period from 1965 to 2005. The data was carefully quality controlled, with only years included that had less than 15% of the within-year record classified as missing (including both 'missing' and

'accumulation' flags), as well as only including stations with less than 5 years missing. Furthermore, annual cumulative precipitation plots for the sub-daily record were compared visually with the annual cumulative plots for the daily-read gauged record collected at the same location, and years for which the annual cumulative rainfall from the sub-daily gauges departed from the annual cumulative rainfall from the daily gauges by more than 15% were also classified as 'missing'. This filtering process yielded a total of 35 stations in Australia with an average of 5.6% of years missing throughout the record across all stations, with locations shown in **Figure 3**. Due to the sparse sampling of data throughout most of the Australian continent, only the east Australian (EA) region was considered in this analysis (comprising 30 stations), with the domain shown in **Figure 3**. At each station, series of annual (block) maxima were derived for durations from 6 minutes through to 72 hours.

INSERT FIGURE 3 HERE

[26] The second precipitation dataset was the longer and more complete record obtained from a quality-controlled daily-read dataset from 1910 to 2005, described more fully in [*Haylock and Nicholls*, 2000; *Lavery et al.*, 1992]. As described in these papers, the quality control undertaken for this particular dataset included: investigation of the station history documentation to remove stations with changes to observing practices, changes in the exposure of the rain gauge, changes in rain gauge type, together with detailed statistical testing to check station integrity.

[27] In more than 95% of cases, the station sites of the daily-read gauges were at different locations to the sites for the sub-daily gauges described above, such that this dataset is largely independent of the sub-daily dataset and therefore can be used as an independent means of evaluating the sub-daily results. Only stations with less than 10% of years classified as 'missing' were considered, totalling 93 stations, with an average of 3.8% of years classified as missing across all the stations. Due to the larger number of locations for daily data, the southwest Western Australia (SWWA) and southeast Australia (SEA) regions defined in **Figure 3** were also analysed in addition to the SE region considered for the sub-daily dataset.

[28] Dealing with missing data in all cases is difficult, and in particular in the case of the sub-daily record for which there are limited sub-daily gauges nearby from which to infill. As such, the primary quality control measure used here was to minimise the number of years classified as missing. Of the data that was missing, three alternative infilling techniques were

adopted. The first involved substituting the mean annual maxima for that year across all the remaining locations where data was available, after adjusting for the station mean. The second technique involved substituting the mean annual maxima at that station across all years with data. Finally a stochastic infilling technique was used in which annual maxima were drawn from other years at the same station. Although none of these infilling techniques can expected to result in an accurate estimate of annual maximum precipitation for the missing years, the use of three alternative techniques allows testing of the robustness of the results described in subsequent sections to different treatments of missing data. In all cases, the different infilling approaches did not make any substantive differences to any of the results presented, with this being due to the relatively small number of records missing and the benefits of using multiple spatial locations to limit the reliance on individual data points. The results presented in the subsequent section are those derived using the first infilling method.

[29] Of greater concern is the potential for inherent measurement biases in rainfall gauging. In particular, the sub-daily rainfall gauges were replaced at many locations throughout Australia in the 1990s and early 2000s, with the most common instrument change being from a Dines pluviograph recorder to a Tipping Bucket Rain Gauge (TBRG). A detailed inventory of gauge changes at each station was obtained from the Australian Bureau of Meteorology, and two alternative approaches were considered to test whether such gauge changes influenced the results. In the first approach, a univariate non-stationary GEV model with both trend and step-change covariates was applied at each location (without consideration of whether the trend or step change was statistically significant), with the date of the step change selected based on the recorded date of the gauge change. Of the 30 sub-daily stations, step changes at 17 of the locations were positive (suggesting that the trend after accounting for the step change is smaller than by ignoring the step change), with step changes at the remaining 13 locations being negative. This result alone suggests the impact of the step change on the trend results is likely to be minor, as one would expect any systematic biases due to shifting from the Dines to the TBRG should result in step changes of the same sign and similar magnitude. As a further means of evaluating the implication of any systemic effects due to gauge changes, these step changes were then removed from each univariate time series, and the max-stable process model was fitted to this adjusted data. The results from this analysis were almost identical to the case where the step change was not accounted for. Finally, the spatial GEV model was applied using only data from 1965-1990 (with this data being almost

completely before any instrumentation change) and the results were consistent with the longer records except for wider confidence intervals due to the shorter record length. This analysis shows that the implications of gauge changes do not appear to have any notable impact on the results and conclusions presented in this paper, and therefore the remaining analysis uses the complete record without explicitly modelling the implications of any gauge changes.

[30] Finally, four separate temporal covariates were considered. The first represents a linear trend, which is simply constructed as the sequence from zero to the number of observations minus one. The second comprises a time series of average Australian annual land surface temperature, obtained from the Australian Bureau of Meteorology (http://www.bom.gov.au/cgi- bin/silo/cli_var/area_timeseries.pl). Here, this is used as a surrogate of the land-surface temperature trend at the time of the storm event [*Hardwick-Jones et al.*, 2010; *Lenderink and van Meijgaard*, 2008], due to the difficulties in averaging land-surface temperature prior to each storm event when considering annual maxima at multiple locations. The third represents the global average sea surface temperature time series obtained from the International Comprehensive Ocean-Atmosphere Data Set (ICCODS) sea surface temperature anomaly record (http://jisao.washington.edu/data/global_sstanomts/), and is used as a surrogate for the temperature of the moisture source region as discussed in [*Hardwick-Jones et al.*, 2010]. Finally, the Southern Oscillation Index (SOI) is used as a measure of the El Niño-Southern Oscillation (ENSO) phenomenon, and was obtained from the Australian Bureau of Meteorology website (http://www.bom.gov.au/climate/current/soihtm1.shtml). With the exception of the linear trend, each covariate is plotted from 1910 to 2005 in **Figure 4**.

INSERT FIGURE 4 HERE

4. Results

[31] We now apply the max-stable process model described in Section 2, to both the sub-daily rainfall data for the east Australian domain, as well as the longer daily data record in each of the three domains shown in **Figure 3**. The results of these analyses are described in turn below.

4.1 Sub-daily rainfall

[32] We commence by considering the sub-daily precipitation observations at multiple point locations in eastern Australia. By way of a preliminary analysis, we fit a non-stationary univariate GEV model using a linear trend as the covariate as described in [*Coles*, 2001] to each of the gauged locations, and then evaluate both the sign and the significance of this trend. These results are shown for the 6-minute data in **Figure 5,** with red (blue) indicating downward (upward) trends and filled circles indicating a statistically significant trend at the 10% significance level. As can be seen, although the magnitude of increase in extreme precipitation varies considerably from location to location, there is no clear spatial pattern associated with physiographic features such as coastlines or mountain ranges, nor any clear relationship with major climate zones such as the winter-dominated rainfall patterns in the southern parts of the country, summer-dominated monsoonal rainfall in the north, arid climate in the centre and largely uniform rainfall in the southeast [e.g. see *Gallant et al.*, 2007 for a possible depiction of relevant climate zones for the detection of change to extreme rainfall]. For the remainder of the sub-daily analysis we therefore focus on the east Australian domain as a single homogenous region, as this maximises the number of stations to include in the model.

INSERT FIGURE 5 HERE

[33] The location and scale parameters are modelled spatially as a linear function of longitude, latitude, elevation and distance to coast (including the square root of these variables), with the exact form of model derived using a forward stepwise selection procedure informed by the (composite) likelihood ratio statistic. The shape parameter was modelled uniformly across the domain, and was found to be on average slightly positive (~0.17) with some variation depending on the storm burst duration that was analysed. The models that were selected for each of the rainfall durations are shown in **Table 1**, and highlight that complex combinations of the covariates are required to describe the spatial variability in location and scale parameters. This is expected due to the large area covered by the domain, and alternative formulations of predictors to estimate spatial variability in the GEV parameters are likely to be equally valid. Nevertheless a comparison of the parameters derived from the models given in **Table 1** with the point estimates of the parameters by fitting a univariate GEV model to each location showed reasonable consistency, indicating adequate spatial modelling of the max-stable process parameters. Furthermore, a sensitivity analysis using slightly different sets of spatial covariates did not have a significant impact on

the value of the temporal covariates which are the focus of this study, and therefore the models described in **Table 1** are considered suitable for the ensuing analysis.

[34] The magnitude of the temporal variation of extremes using each of the four covariates is shown in **Figure 6**, using the sub-daily information for durations from 6 minutes to 72 hours. The results using daily data in the east Australian domain from 1965 to 2005 are also provided to check for consistency between the two datasets. The results are presented in terms of: the percentage change from the beginning to the end of the record for the trend covariate (**Figure 6a**); the percentage change per degree change in temperature for the Australian temperature and global sea surface temperature covariates (**Figures 6b** and **6c**); and the percentage change per standard deviation of the southern oscillation index (**Figure 6d**).

INSERT FIGURE 6 HERE

[35] To highlight the implications of spatial correlation, point estimates and confidence bounds were generated assuming that the data are spatially independent (solid and dotted blue lines), or modelling spatial dependence using the Gaussian extreme value process model of [*Smith*, 1990] (solid and dotted red lines). The 90% confidence intervals were estimated using the profile likelihood, with the likelihood statistics adjusted appropriately using the approach described by [*Rotnitzky and Jewell*, 1990] due to the misspecification of the likelihood function [*Padoan et al.*, 2010]. As can be seen, in all cases the confidence interval using the max-stable process model was wider than the confidence interval assuming spatial independence, as expected from the results from the synthetic study described earlier. Interestingly, although this effect was small for the sub-daily data, significant difference in confidence intervals could be found for the daily data, highlighting that although more spatial locations are available at the daily scale, this does not necessarily translate to a large increase in information for the max-stable extreme value model.

[36] We now evaluate the implication of different temporal covariates on the east Australian extreme precipitation series. Considering firstly the implications of a linear trend (**Figure 6a**), it can be seen that short duration extreme rainfall has been increasing significantly over the period of record from 1965 to 2005, with the mean annual maximum rainfall at the shortest duration (6-minute) increasing by 18% (10% to 25%). This rate of increase is heavily dependent on storm burst duration, with half hourly annual maxima increasing by 9.9%

(1.4% to 17%) and hourly rainfall increasing by only 4.6% (-3.1% to 12%) over this same period. When looking at 24-hour rainfall, we do not find strong evidence of any trend, and at longer-duration timescales there is some evidence of decreasing annual maximum rainfall. Comparing these results with the daily annual maxima dataset, which as discussed were derived from different types of gauges largely located in different point locations within the same east Australian domain, we find the results to be consistent, with the trend in daily maxima also not being statistically different from zero.

[37] To better understand the nature of these changes, the influence of two temperature-related covariates – Australian annual average temperature (**Figure 6b**) and global sea surface temperature (**Figure 6c**) – were also considered. At the shortest duration, precipitation was found to increase by about 5.6% (-0.7 to 11.0%) per degree of Australian annual average temperature, and 22.5% (10.8 to 33.7%) per degree of global sea surface temperature. Given the increase in Australian annual average temperature has been less than a degree over this period (e.g. CSIRO, 2007), these results show that average annual land surface temperature change does not completely explain the observed increase of 18% over this period as described in the previous paragraph. Furthermore, even at the 6-minute timescale the relationship between extreme precipitation and Australian land surface temperature is not statistically significant at the 5% significance level, suggesting that average annual land surface temperature may be a poor predictor of change to extreme precipitation. In contrast, the global sea surface temperature covariate shows a much stronger relationship, and is significantly different from zero for all sub-hourly durations. Once again, however, the increase in global SST was only about 0.4°C, yielding an expected increase due to SST of about half the rate that has been observed based on the linear trend results. The attribution of the strong increase in sub-daily precipitation therefore remains an area requiring further investigation, potentially with the aid of dynamical modelling approaches to better understand the large-scale atmospheric drivers of short-duration precipitation.

[38] Finally, the southern oscillation index was used as an indicator of the ENSO phenomenon, the leading mode of climate variability affecting Australian rainfall at the inter-annual timescale. The results of this analysis show that the strongest relationship between annual maximum precipitation and the SOI occurs at the daily timescale, with an increase in average 24-hour rainfall of 3.2% (0.97% to 5.4%), and for daily rainfall of 4.6% (2.3% to 7.1%) per standard deviation of the SOI. Interestingly, the relationship weakens for shorter

durations, and is no longer statistically significant for durations below about 3 hours, suggesting that the SOI is most influential for longer-duration storm events.

4.2 Daily rainfall

[39] Although results from the daily rainfall record were presented for east Australian data in the previous section, this was only based on information from 1965 to 2005 to ensure consistency with the sub-daily record. Here we consider the full record from 1910 to 2005 for east Australia, as well as two other regions shown in **Figure 3**. Only the results using the max-stable process model are presented here, as the spatially independent extreme value model is not likely to be realistic for the more densely gauged daily data.

[40] The results for the Australian temperature trend, global SST trend and the SOI are presented in **Table 2**. The linear trend was not considered here as a linear change is expected to be a poor representation of change to precipitation data over such a long period. Considering east Australia, the results are consistent with the results presented in **Figure 6** for each of the indices, with an absence of a statistically significant relationship between daily annual maximum rainfall and Australian average temperature and the globally averaged SST field, and with a statistically significant increase of annual maximum rainfall of 2.8% per standard deviation of the SOI. The confidence intervals are approximately half as wide as compared to those shown in **Figure 6**, highlighting the benefits of considering longer data in providing more precise statistical inferences.

[41] Considering the remaining locations, it can be seen that there is a decrease in annual maximum precipitation as a function of Australian temperature which is not statistically significant in southeast Australia but is significant at the 90% level in southwest Western Australia. This confirms the results of other studies such as [*Alexander et al.*, 2007; *Gallant et al.*, 2007] who suggest that extremes in daily rainfall may be decreasing in areas where there are large decreases in mean annual rainfall, with such decreases having been observed in southwest Western Australia.

[42] Finally, there is a negative, but statistically insignificant, relationship with global SST at all locations, and a positive and statistically significant relationship with the SOI, suggesting that the SOI exerts a small but statistically significant influence on extreme daily rainfall in all the regions analysed.

Conclusions

[43] In this paper we present one of the first applications of a non-stationary generalised extreme value model based on max-stable process theory, in which data-level and parameter-level dependence between precipitation data at individual point locations is explicitly accounted for within the modelling framework. The advantages of such a modelling framework were shown using a synthetic example, in which the probability of detecting a statistically significant trend in the location parameter was evaluated for a range of record lengths, number of spatial locations, and spatial dependence. In particular, the inclusion of numerous spatial locations resulted in significant increases in the probability of being able to detect a statistically significant trend, particularly when data-level dependence was low. As data-level dependence increases, the max-stable process model was able to account for the decrease in information via wider confidence intervals, whereas the spatial GEV model would have resulted in unrealistically high levels of confidence in any temporal trends.

[44] Using this method, it was possible to detect a strong, statistically significant trend in sub-daily (and particularly sub-hourly) precipitation across eastern Australia, with these increases contrasting with the absence of any statistically significant changes at the daily timescale. This finding is unsurprising for several reasons. Firstly, as described earlier the temperature scaling of extreme precipitation in Australia also shows very different behaviour for short-duration precipitation compared with daily precipitation, with maximum sensitivity with surface temperature also occurring for sub-hourly durations [*Hardwick-Jones et al.*, 2010]. Furthermore, the sub-hourly timescale is generally regarded as the timescale for individual convective cells within thunderstorm systems [*Wallace and Hobbs*, 2006], and thus is the timescale which would be most sensitive to the moisture holding capacity of the atmosphere. Finally, international studies using regional climate models also have found much stronger scaling for hourly compared with daily precipitation [e.g. *Hanel and Buishand*, 2010].

[45] At the daily timescale, no change in annual maximum rainfall could be detected with the exception of southwest Western Australia, where a 7.4% decrease in annual maximum rainfall per degree of land surface temperature was detected. Although the choice of suitable covariates to use for this type of analysis is likely to be debatable, the conclusions are generally consistent with other studies which show an absence of significant changes to extreme daily rainfall in most locations around Australia except for locations where the annual rainfall is decreasing strongly, most notably southwest Western Australia [*Alexander*

et al., 2007; *Gallant et al.*, 2007]. Finally, this study showed that although the influence of ENSO on annual maximum rainfall in Australia is small, it is nonetheless detectable using the max-stable process model described here.

[46] These results therefore affirm the importance of understanding changes in precipitation at all timescales, and in particular at the scales of individual storm events rather than the daily timescale for which data is more readily available. Although the availability of sub-daily data in Australia is generally limited (with most records being too short, containing large quantities of missing data, and including numerous changes to instrumentation which might bias the results), making the application of this data for climate studies difficult, this paper highlights that a careful statistical analysis that explicitly accounts for the spatial nature of rainfall data, will be beneficial in recovering useful information from such an instrumental record.

ACKNOWLEDGEMENTS

[47] We wish to acknowledge Dr Mathieu Ribatet for making the *SpatialExtremes* package available in R, and for including temporal covariates in this package for this study. The rainfall data was provided by the Australian Bureau of Meteorology and we wish to acknowledge Dr S ri S rikanthan's a ssistance in a nswering questions ab out the sub-daily instrumentation. SAS is supported by the Australian Research Council under the Discovery Project scheme (DP0877432).

<u>References</u>

Alexander, L., P. Hope, D. Collins, B. Trewin, A. Lynch, and N. Nicholls (2007), Trends in Australia's climate means and extremes: a global context, *Australian Meteorological Magazine*, *56*, 1-18.
Alexander, L., et al. (2006), Global observed changes in daily climatic extremes of temperature and precipitation, *Journal of Geophysical Research*, *111*(D05101).
Allan, R. P., and B. J. Soden (2008), Atmospheric warming and the amplification of precipitation extremes, *Science*, *321*, 1481-1484.
Allan, R. P., B. J. Soden, V. O. John, W. Ingram, and P. Good (2010), Current changes in tropical precipitation, *Environmental Research Letters*, *5*(025205).
Aryal, S. K., B. C. Bates, E. P. Campbell, Y. Li, M. J. Palmer, and N. R. Viney (2009), Characterizing and Modelling Temporal and Spatial Trends in Rainfall Extremes, *Journal of Hydrometeorology*, *10*, 13.
Berne, A., G. Delrieu, J. D. Creutin, and C. Obled (2004), Temporal and spatial resolution of rainfall measurements required for urban hydrology, *Journal of Hydrology*, *299*, 166-179.
Buishand, A. T. (1991), Extreme rainfall estimation by combining data from several sites, *Hydrological Sciences Journal*, *36*(4).

Coles, S. G. (1993), Regional modelling of extreme storms via max-stable processes, *Journal of the Royal Statistical Society Series B*, *55*, 797-816.

Coles, S. G. (2001), *An Introduction to Statistical Modelling of Extreme Values*, 208 pp., Springer, London.

Coles, S. G., L. R. Pericchi, and S. A. Sisson (2003), A fully probabilistic approach to extreme value modelling, *Journal of Hydrology*, *273*, 35-50.

de Haan, L. (1984), A Spectral Representation for Max-Stable Processes, *The Annals of Probability*, 1194-1204.

de Haan, L., and S. Resnick (1977), Limit theory for multivariate sample extremes, *Z. Wahrscheinlichkeitstheorie verw. Gebiete*, *40*, 317-337.

de Haan, L., and J. Pickands (1986), Stationary Min-Stable Stochastic Processes, *Probability Theory and Related Fields*, *74*(477-492).

de Haan, L., and T. T. Pereira (2006), Spatial extremes: Models for the stationary case, *The Annals of Statistics*, *34*, 146-168.

Fowler, H. J., and R. L. Wilby (2010), Detecting changes in seasonal precipitation extremes using regional climate model projections: Implications for managing fluvial flood risk, *Water Resources Research*, *46*(W03525).

Frei, C., and C. Schar (2001), Detection probability of trends in rare events: theory and application to heavy precipitation in the alpine region, *Journal of Climate*, *14*, 1568-1584.

Frich, P., L. Alexander, P. Della-Marta, B. Gleason, M. Haylock, A. M. G. Klein Tank, and T. C. Peterson (2002), Observed coherent changes in climatic extremes during the second half of the twentieth century, *Climate Research*, *19*, 193-212.

Gallant, A., K. J. Hennessy, and J. Risbey (2007), Trends in rainfall indices for six Australian regions: 1910-2005, *Australian Meteorological Magazine*, *56*, 223-239.

Groisman, P. Y., R. W. Knight, D. R. Easterling, T. R. Karl, G. C. Hegerl, and V. N. Razuvaev (2005), Trends in intense precipitation in the climate record, *Journal of Climate*, *18*, 1326-1350.

Haerter, J. O., P. Berg, and S. Hagemann (2010), Heavy rain intensity distributions on varying time scales and at different temperatures, *Journal of Geophysical Research*, *115*(D17102).

Hanel, M., and T. A. Buishand (2010), On the value of hourly precipitation extremes in regional climate model simulations, *Journal of Hydrology*, *393*(3-4), 265-273.

Hardwick-Jones, R., S. Westra, and A. Sharma (2010), Observed relationships between extreme sub-daily precipitation, surface temperature and relative humidity, *Geophysical Research Letters*, *37*(L22805).

Haylock, M., and N. Nicholls (2000), Trends in extreme rainfall indices for an updated high quality data set for Australia, 1910-1998, *International Journal of Climatology*, *20*(13), 1533-1541.

Hegerl, G. C., F. Zwiers, V. V. Kharin, and P. A. Stott (2004), Detectability of anthropogenic changes in temperature and precipitation extremes, *Journal of Climate*, *17*, 3683-3700.

Hosking, J. R. M., J. R. Wallis, and E. F. Wood (1985), Estimation of the generalized extreme-value distribution by the method of probability-weighted moments, *Technometrics 27*, 251-261.

IPCC (2007), Summary for Policymakers*Rep.*, Cambridge Univeristy Press, Cambridge, United Kingdom.

Jenkinson, A. F. (1955), The frequency distribution of the annual maximum (or minimum) values of meteorological elements, *Quarterly Journal of the Royal Meteorological Society*, *87*, 158-171.

Katz, R. W. (2010), Statistics of extremes in climate change, *Climatic Change*, *100*, 71-76.

Katz, R. W., M. B. Parlange, and P. Naveau (2002), Statistics of extremes in hydrology, *Advances in Water Resources*, *25*, 18.

Kharin, V. V., and F. Zwiers (2000), Changes in the extremes of an ensemble of transient climate simulations with a coupled atmosphere-ocean GCM, *Journal of Climate*, *13*, 3760-3788.

Lavery, B., A. Kariko, and N. Nicholls (1992), A historical rainfall dataset for Australia, *Australian Meteorological Magazine*, *40*, 33-39.

Leadbetter, M. R., G. Lindgren, and H. Rootzen (1983), *Extremes and related properties of random sequences and processes*, Springer-Verlag, New York.

Lenderink, G., and E. van Meijgaard (2008), Increase in hourly precipitation extremes beyond expectations from temperature changes, *Nature Geoscience*, *1*, 511-514.

Min, S. K., X. Zhang, F. W. Zwiers, P. Friederichs, and A. Hense (2009), Signal detectability in extreme precipitation changes assessed from twentieth century climate simulations, *Climate Dynamics*, *32*, 95-111.

O'Gorman, P. A., and T. Schneider (2009), The physical basis for increases in precipitation extremes in simulations of 21st-century climate change, *Proceedings of the National Academy of Sciences*, *106*(35), 14773-14777.

Padoan, S. A., M. Ribatet, and S. A. Sisson (2010), Likelihood-based inference for max-stable processes, *Journal of the American Statistical Association*, *105*, 263-277.

Perkins, S. E., A. J. Pitman, and S. A. Sisson (2009), Smaller projected increases in the 20-year temperature returns over Australia in skill-selected climate models, *Geophysical Research Letters*, *36*(L06710).

Resnick, S. (1987), *Extreme Values, Point Processes and Regular Variation*, Springer Verlag, New York.

Rotnitzky, A., and N. P. Jewell (1990), Hypothesis testing of regression parameters in semiparametric generalised linear models for cluster correlated data, *Biometrika*, *77*, 485-497.

Sang, H., and A. E. Gelfand (2007), Hierarchical modeling for extreme values observed over space and time, *Environmental and Ecological Statistics*, *16*, 406-426.

Schlather, M. (2002), Models for stationary random fields, *Extremes*, *5*, 33-44.

Schlather, M., and J. A. Tawn (2003), A dependence measure for multivariate and spatial extreme values: Properties and inference, *Biometrika*, *90*, 139-154.

Sisson, S. A., L. R. Pericchi, and S. G. Coles (2006), A case for a reassessment of the risk of extreme hydrological hazards in the Caribbean, *Stochastic Environmental Research and Risk Assessment*, *20*, 296-306.

Smith, T. F. (1990), Max-stable processes and spatial extremes, *Unpublished manuscipt*.

Trenberth, K. E., A. Dai, R. M. Rasmussen, and D. B. Parsons (2003), The changing character of precipitation, *Bulletin of the American Meteorological Society*, *84*, 1205-1217.

von Mises, R. (1954), La distribution de la plus grande de n valeurs, in *American Mathematical Society*, edited, pp. 271-294, Providence, Rhode Island, USA.

Wallace, J. M., and P. V. Hobbs (2006), *Atmospheric Science: An Introductory Survey*, 2nd edition ed.

Westra, S., R. Mehrotra, A. Sharma, and R. Srikanthan (2010), Continuous Rainfall Simulation: 2 - A regionalised sub-daily disaggregation approach, *Water Resources Research (submitted manuscipt)*.

Wilbanks, T. J., P. Romero Lankao, M. Bao, F. Berkhout, S. Cairncross, J. P. Ceron, M. Kapshe, R. Muir-Wood, and R. Zapata-Mari (2007), Industry, settlement and society*Rep.*, 357-390 pp, Cambridge, UK.

Zhang, X., F. W. Zwiers, and G. Li (2004), Monte Carlo Experiments on the Detection of Trends in Extreme Values, *Journal of Climate*, *17*, 1945-1952.

Zhao, X., and P.-S. Chu (2010), Bayesian changepoint analysis for extreme events (typhoons, heavy rainfall and heat waves): An RJMCMC approach, *Journal of Climate*, *23*, 1034-1046.

Tables

Table 1: Covariates used for spatial model, selected via a forward selection approach using a likelihood ratio test. Predictors include latitude, longitude, elevation and distance to coast, and the square root of these variables.

Storm burst duration	Model
6 min	$\mu(x) = \alpha_0 + \alpha_1(\text{lat}) + \alpha_2(\text{lon}) + \alpha_3(\text{lon}^{1/2})$ $\sigma(x) = \beta_0 + \beta_1(\text{lat})$ $\xi(x) = \gamma_0$
12 min	$\mu(x) = \alpha_0 + \alpha_1(\text{lat}) + \alpha_2(\text{lon}^{1/2}) + \alpha_3(\text{lon}) + \alpha_4(\text{dist})$ $\sigma(x) = \beta_0 + \beta_1(\text{lat}) + \beta_2(\text{lon}^{1/2}) + \beta_3(\text{dist})$ $\xi(x) = \gamma_0$
30 min	$\mu(x) = \alpha_0 + \alpha_1(\text{lat}) + \alpha_2(\text{lon}^{1/2}) + \alpha_3(\text{lon}) + \alpha_4(\text{dist})$ $\sigma(x) = \beta_0 + \beta_1(\text{lat}) + \beta_2(\text{lon})$ $\xi(x) = \gamma_0$
1 hr	$\mu(x) = \alpha_0 + \alpha_1(\text{lat}^{1/2}) + \alpha_2(\text{lon}^{1/2}) + \alpha_3(\text{dist}^{1/2}) + \alpha_4(\text{lat})$ $\sigma(x) = \beta_0 + \beta_1(\text{lat}) + \beta_2(\text{lon}^{1/2})$ $\xi(x) = \gamma_0$
3 hr	$\mu(x) = \alpha_0 + \alpha_1(\text{lat}) + \alpha_2(\text{dist}) + \alpha_3(\text{lon})$ $\sigma(x) = \beta_0 + \beta_1(\text{lat}) + \beta_2(\text{dist}^{1/2}) + \beta_3(\text{lon}^{1/2})$ $\xi(x) = \gamma_0$
24 hr	$\mu(x) = \alpha_0 + \alpha_1(\text{lat}^{1/2}) + \alpha_2(\text{lon}^{1/2}) + \alpha_3(\text{dist}^{1/2}) + \alpha_4(\text{elev}^{1/2})$ $\sigma(x) = \beta_0 + \beta_1(\text{lat}) + \beta_2(\text{dist}^{1/2}) + \beta_3(\text{lon}^{1/2})$ $\xi(x) = \gamma_0$
72 hr	$\mu(x) = \alpha_0 + \alpha_1(\text{lat}^{1/2}) + \alpha_2(\text{lon}) + \alpha_3(\text{dist}^{1/2}) + \alpha_4(\text{elev})$ $\sigma(x) = \beta_0 + \beta_1(\text{lat}^{1/2}) + \beta_2(\text{dist}^{1/2}) + \beta_2(\text{lon}^{1/2})$ $\xi(x) = \gamma_0$

Table 2: Relationship between daily rainfall from 1910-2005 and three covariates: Australian temperature, Global sea surface temperature (SST), and the Southern Oscillation Index (SOI). Relationship with temperature covariates is expressed as percentage change per degree change in the covariate, while relationship with SOI is expressed per standard deviation of the SOI. Numbers in parentheses represent the 5% and 95% confidence limits calculated using profile likelihood.

	Australian Temperature	Global SST	SOI
Eastern Australia	-1.6 (-5.9 to 2.87)	-0.25 (-4.6 to 4.3)	2.8 (1.2 to 4.3)
Southeast Australia	-2.6 (-6.5 to 1.5)	-0.83 (-5.4 to 3.4)	2.0 (0.05 to 3.8)
Southwest Western Australia	-7.4 (-13.0 to 0.0)	-1.3 (-8.7 to 5.8)	2.6 (0.17 to 5.2)

List of Figure Captions

Figure 1: Max-stable processes $Z(s)$ in one and two dimensions based on a Gaussian storm profile. Panel (a) illustrates $n = 5$ Gaussian "storms" in one dimension (grey lines) with the process maxima outlined in black. Panel (b) illustrates a max-stable process in two dimensions $s = (s_1, s_2)$ with a positively correlated Gaussian storm profile.

Figure 2: Probability of finding β_1 to be statistically significant at the 5% significance level. (a) Implications of different sample lengths n, with different percentage change of detection (i.e. 50%, 95% and 99% chance of detecting a statistically significant trend), and different values of ξ; (b) implications of ξ assuming 50% chance of detection; (c) implications of number of spatial locations assuming sample length $n = 100$, assuming differing degrees of spatial dependence, assuming 50% chance of detecting a statistically significant trend; and (d) as with (c) but assuming 95% change of detecting a statistically significant trend.

Figure 3: Location of quality-controlled pluviograph (blue dots) and daily-read (gray dots) stations. The spatial extremes analysis was conducted for three regions for the daily data: southwestern Western Australia (SWWA), southeast Australia (SEA) and eastern Australia (EA), and for EA only for pluviograph data due to limited sampling density elsewhere.

Figure 4: Covariates used in the study.

Figure 5: Non-stationary univariate GEV model with a linear trend as covariate applied to each station for 6-minute annual maximum pluviograph data (left panel) from 1965 to 2005, and the daily dataset (right panel) from 1910 to 2005. Red and blue indicate downward and upward trends, respectively, with filled circles indicating the trend is statistically significant at the 10% significance level.

Figure 6: Relationship between sub-daily precipitation across east Australia for durations from 6 minutes through to 72 hours, and the three temporal covariates. Solid blue line represents the results from a spatial GEV model (ignoring spatial dependence), while solid orange line represents results from max-stable model using the Smith spatial dependence function. Dotted lines represent the 95% confidence interval. The outcomes from the daily model is also shown (slightly offset for visual purposes), including red dots (spatial GEV) and green dots (max-stable distribution), together with associated 95% confidence interval.

Figure1

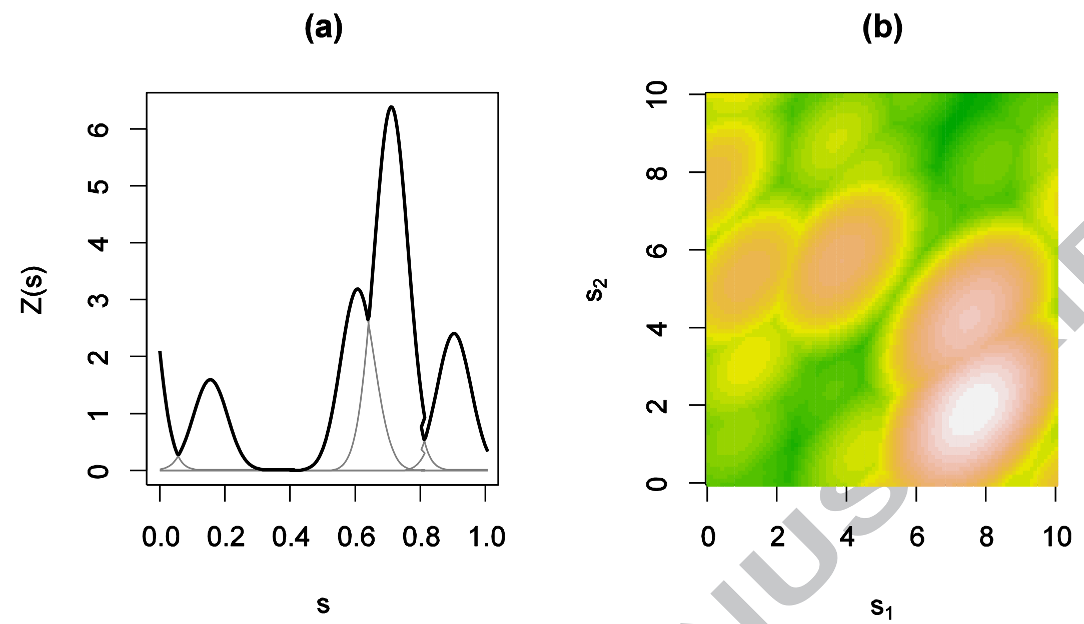

Figure2

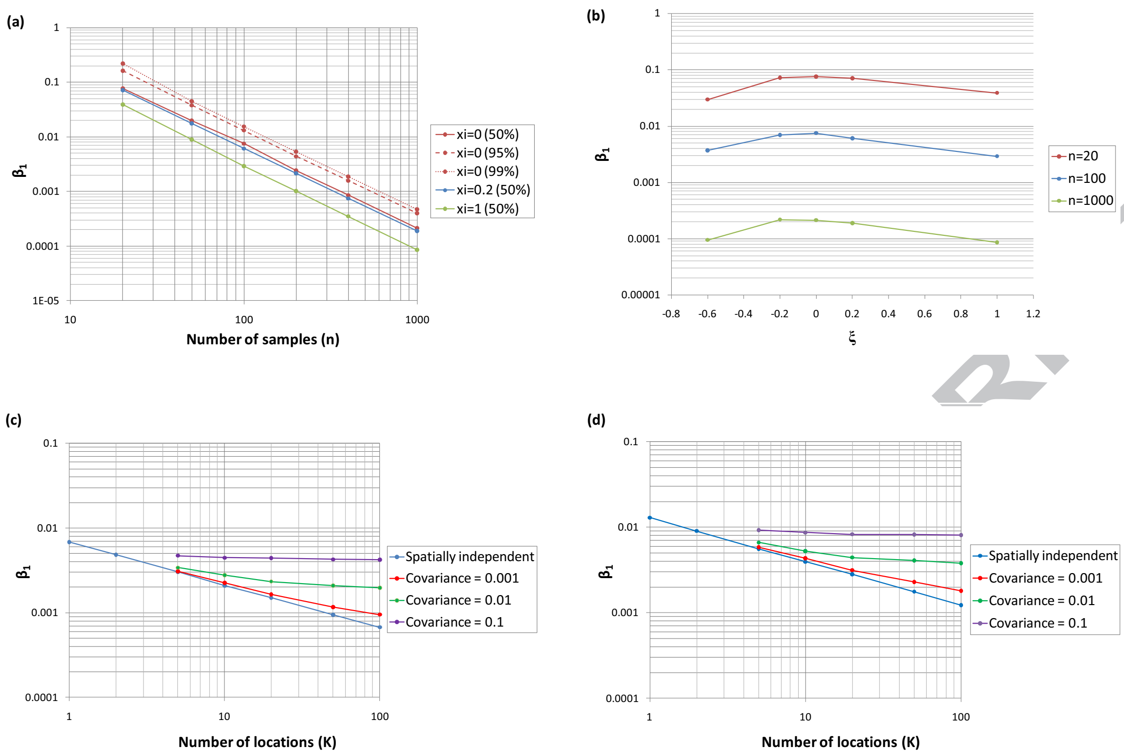

(a)
1
0.1
0.01
0.001
0.0001
1E-05
β_1
10
100
1000
Number of samples (n)
xi=0 (50%)
xi=0 (95%)
xi=0 (99%)
xi=0.2 (50%)
xi=1 (50%)
(b)
1
0.1
0.01
0.001
0.0001
0.00001
β_1
-0.8
-0.6
-0.4
-0.2
0
0.2
0.4
0.6
0.8
1
1.2
ξ
n=20
n=100
n=1000
(c)
0.1
0.01
0.001
0.0001
β_1
1
10
100
Number of locations (K)
Spatially independent
Covariance = 0.001
Covariance = 0.01
Covariance = 0.1
(d)
0.1
0.01
0.001
0.0001
β_1
1
10
100
Number of locations (K)
Spatially independent
Covariance = 0.001
Covariance = 0.01
Covariance = 0.1

Figure3

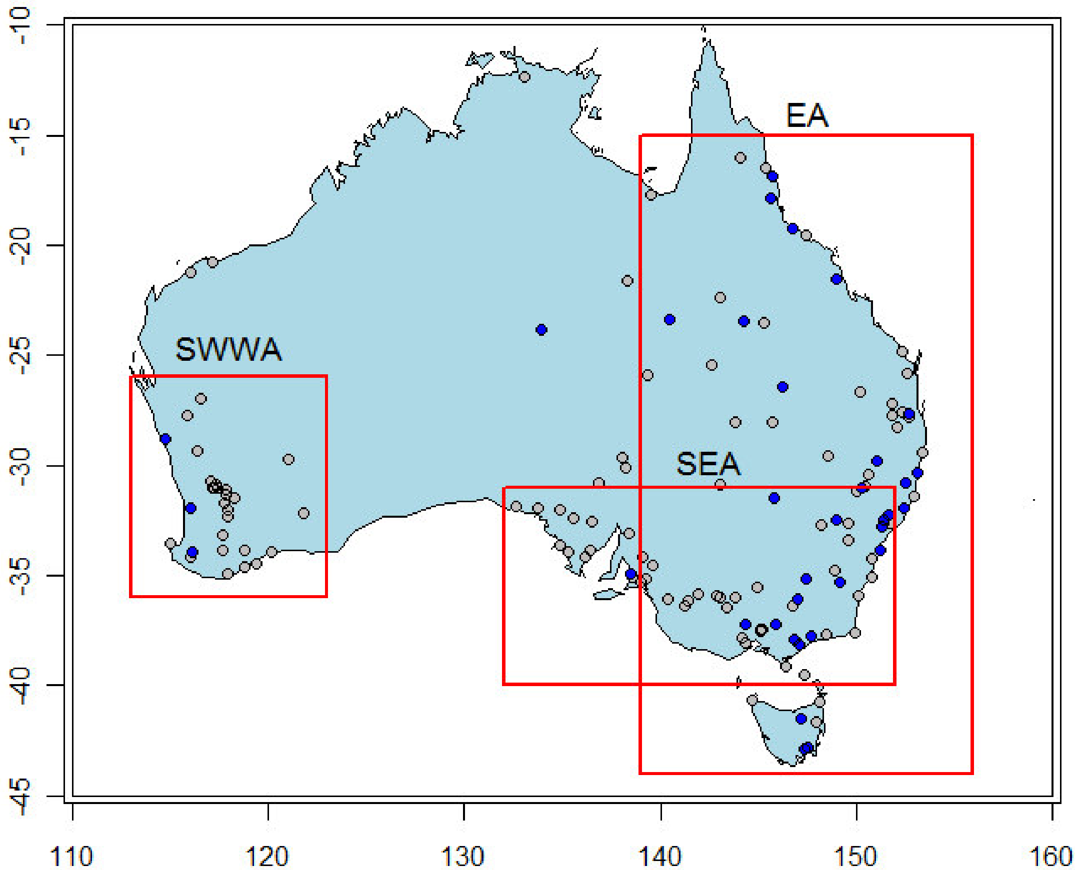

Figure4

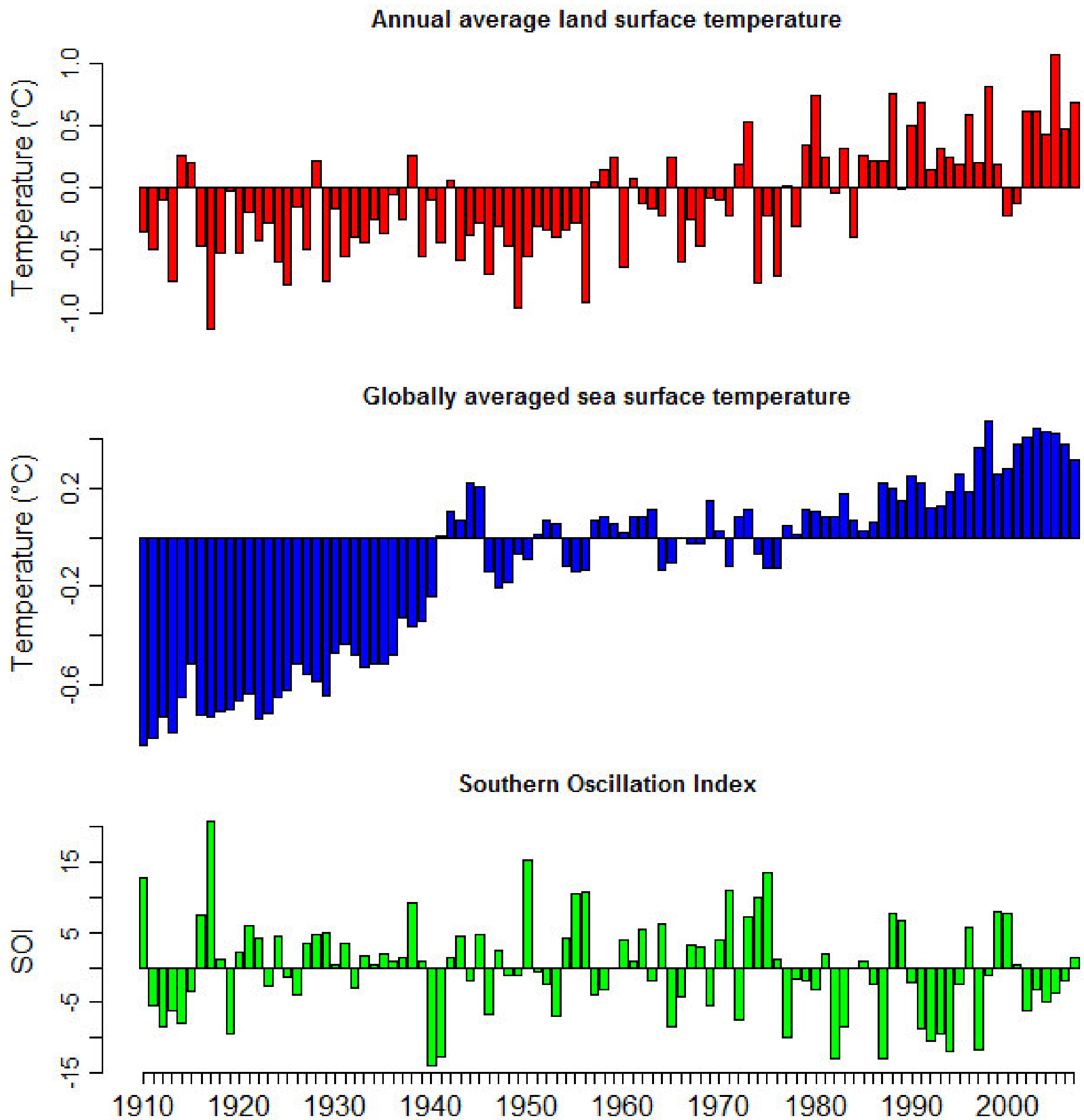
Annual average land surface temperature
Temperature (°C)
-1.0
-0.5
0.0
0.5
1.0
Globally averaged sea surface temperature
Temperature (°C)
-0.6
-0.2
0.2
Southern Oscillation Index
SOI
-15
-5
5
15
1910
1920
1930
1940
1950
1960
1970
1980
1990
2000

Figure5

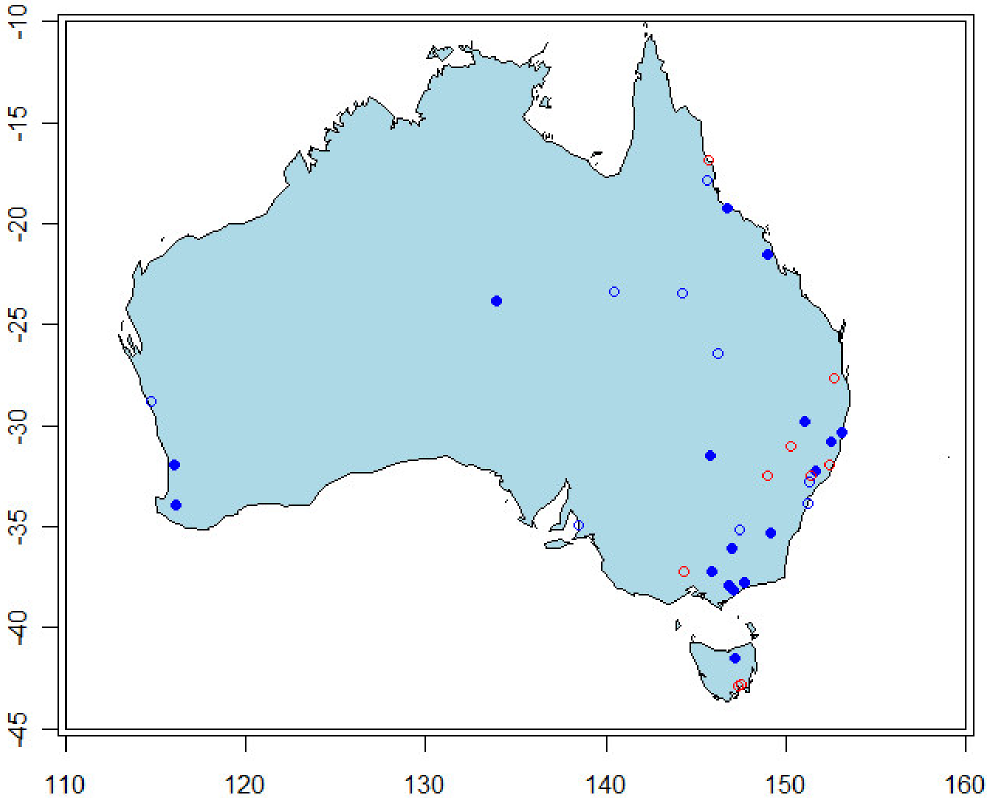

Figure6

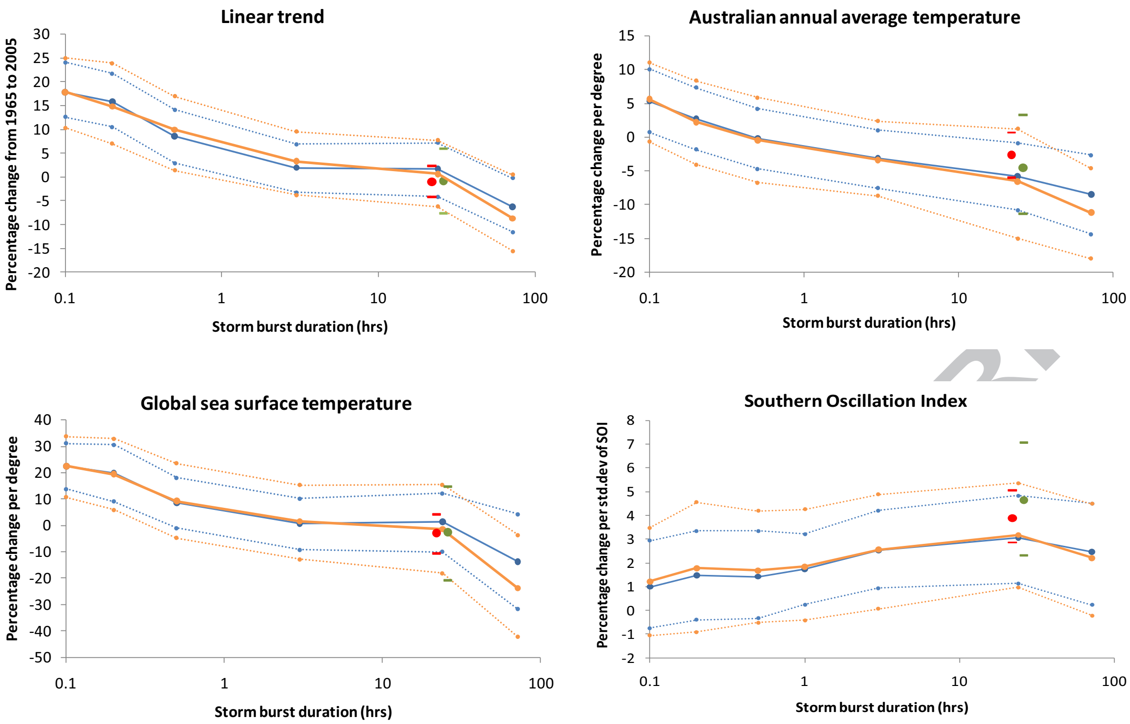
Linear trend
Percentage change from 1965 to 2005
Storm burst duration (hrs)
Australian annual average temperature
Percentage change per degree
Storm burst duration (hrs)
Global sea surface temperature
Percentage change per degree
Storm burst duration (hrs)
Southern Oscillation Index
Percentage change per std.dev of SOI
Storm burst duration (hrs)

Research Highlights

- We demonstrate application of a max-stable process model using extreme rainfall data.
- We show how this model improves precision of inference by including spatial information.
- We find strong increases in sub-hourly extreme precipitation in East Australia.
- We find limited change to daily rainfall, except for a decrease in SW Australia.